


Y. Y. FEI  
P. THOMAS  
X. D. ZHU 

# Adsorption and desorption of hydrogen on bare and Xe-covered Cu(111)

Department of Physics, University of California, Davis, CA 95616, USA

Received: 18 April 2006 / Accepted: 25 September 2006  
© Springer-Verlag 2006

**ABSTRACT** Using polarization-modulated ellipsometry to monitor adsorbate coverage in-situ, we studied the activated adsorption of filament-heated molecular hydrogen on Cu(111) and subsequent isothermal desorption of hydrogen adatoms. The adsorption is characterized by a zeroth-order kinetic with a constant sticking probability of  $S_0 = 0.0062$  up to  $\theta = 0.25$ , followed by a Langmuir kinetic until the saturation coverage  $\theta_s = 0.5$  is reached. The desorption follows a second-order kinetic with an activation energy of 0.63 eV and a pre-exponential factor of  $1 \times 10^9$  /s. A pre-adsorbed monolayer of Xe atoms on Cu(111), with a desorption activation energy of 0.25 eV and a pre-exponential factor of  $8 \times 10^{14}$  /s, efficiently blocks the subsequent adsorption of hot molecular hydrogen, making physisorbed Xe useful as templates for spatial patterning of hydrogen adatom density on Cu(111).

PACS 68.43.Jk; 78.68.+m; 81.15.-z; 82.40.Np

## 1 Introduction

Adsorption of hydrogen and rare gas on metals serves as useful models of gas-solid interaction. Depending upon the substrate, adsorption of gaseous hydrogen molecules varies from being weakly activated (e.g.,  $H_2/Ni$ ) to being strongly activated (e.g.,  $H_2/Cu$ ) [1–11]. More readily than other atoms, hydrogen adatoms may, under suitable conditions, reside in the sub-surface region with relative stability or become absorbed into the bulk. From a theoretical perspective the precise determination of binding sites and binding energies of hydrogen atoms and rare gas atoms continues to challenge the first-principle theories of solid surfaces [12]. Furthermore small masses of hydrogen and its isotopic family make them ideal candidates for investigating quantum dissipation effect on mass transport on metals, where the roles of phonons, conduction electrons, disorders, and dimensionality may be systematically explored [13–19]. Cao and coworkers recently reported an experimental study of surface diffusion of hydrogen on Ni(111), using the method of linear diffractions off hydrogen density gratings, and observed the crossover from classical over-barrier hopping to quantum

under-barrier tunneling [20]. The present experimental study is motivated by the interest in extending the study of quantum tunneling diffusion to hydrogen on Cu(111) and Cu(100). The first few steps of such an investigation are controlled adsorption, desorption, and spatial patterning of hydrogen adatoms on Cu. These are the subjects of investigation in this paper.

Adsorption of hydrogen molecules on Cu is known to be an activated process as found out in early studies of gas adsorption on evaporated films [5]. Using supersonic molecular beams as the source, Balooch, Cardillo, Miller, and Stickney attempted the first quantitative measurements of energy barriers for adsorption of molecular hydrogen and deuterium on single-crystal Cu surfaces:  $\sim 5$  kcal/mol on Cu(100) and  $\sim 3$  kcal/mol on Cu(110) [6]. Later using vibrationally hot and translationally/rotationally cold molecular beams, Hayden and Lamont revisited activated adsorption of molecular hydrogen on Cu(110) and concluded that the adsorption activation barrier is in fact close to  $\sim 23$  kcal/mol [7, 8]. They pointed out the importance of taking into account the vibrational degree of freedom. Auerbach, Rettner and Michelsen reported similar findings when they revisited adsorption of hydrogen on Cu(111) [9, 10]. Using a combination of a supersonic molecular beam technique and a temperature-programmed thermal desorption technique, Anger, Winkler and Rendulic were able to confirm that activation energies for adsorption of molecular hydrogen and deuterium on Cu(111), Cu(110), and Cu(100) are much larger than  $3 \sim 5$  kcal/mol [11]. Using an absolute calibration method, these authors determined the saturation coverage of hydrogen adatoms on Cu(111) to be  $\theta_s = 0.5$  when hot molecular beams were used for sources of exposure. They also observed that the subsequent thermal desorption of hydrogen adatoms from both Cu(111) and Cu(100) follows a second-order kinetic and originates from a single state. On Cu(111) (relevant to our present investigation), they reported a desorption activation energy of 18 kcal/mol (0.78 eV) and the pre-exponential factor to be  $\sim 3 \times 10^{11}$  /s. More recently Greuter and Plummer studied the adsorption of hot-filament-produced atomic hydrogen on Cu(111) at 180 K using a combination of photoemission and temperature-programmed thermal desorption techniques [21]. They observed two peaks in the thermal desorption spectrum: one major peak near 300 K as observed by Anger et al., and one minor peak near 230 K. Using a nuclear reaction analysis, Lee and coworkers determined that

 Fax: +1-530 752 4717, E-mail: xdzhu@physics.ucdavis.edu

when Cu(111) is exposed to atomic hydrogen, the saturation coverage of adsorbed hydrogen is  $\theta_s = 0.67$  instead of  $\theta_s = 0.5$  [22]. Based on a high resolution electron energy loss study, Lee and Plummer concluded that the major peak in the thermal desorption spectrum came from hydrogen adatoms at threefold hollow sites on Cu(111) with a saturation coverage of  $\theta_s = 0.5$ , and the minor peak originated from hydrogen adatoms residing at subsurface sites [23, 24].

In the present study, we revisit activated adsorption of filament-heated molecular hydrogen on Cu(111). What distinguishes our study from the previous ones are as follows: (1) we use a polarization-modulated double-nulling ellipsometry [25] to measure in real time the coverage of chemisorbed hydrogen adatoms and physisorbed Xe atoms on Cu(111) so that adsorption and desorption kinetics of both adsorbates are followed directly; (2) we use a filament-heated molecular hydrogen source monitored by a quadrupole mass spectrometer so that we can produce either hot molecular hydrogen or a mixture of atomic hydrogen fragments and hot molecular hydrogen with definable partial pressures; (3) we investigate the blocking effect of physisorbed Xe adatoms on subsequent adsorption of molecular hydrogen and the usefulness of such an effect for spatial patterning of hydrogen adatom density on Cu(111) and other Cu surfaces.

## 2 Experimental procedures

The experiment is carried out in an ultrahigh vacuum chamber with a base pressure of  $2 \times 10^{-10}$  Torr. The chamber is equipped with a 400 liter/s ion pump, an Omicron rear-view low energy electron diffraction (LEED) system, an Omicron Auger electron spectrometer (AES), a UTI 100C quadrupole mass spectrometer (QMS), and an oblique-incidence optical reflectivity difference (OI-RD) measurement system. A 10 mm diameter  $\times$  1.5 mm thick Cu(111) substrate (Surface Preparation Laboratory), is oriented and polished to within  $0.1^\circ$  from the said Miller index plane. Prior to the experiments the substrate is cleaned with cycles of ion sputtering at room temperature for 30 minutes in a  $1 \times 10^{-5}$  Torr Ar-Ne mixture with the ion energy at 1 keV, followed by thermal annealing at 700 K for 10 minutes. After the cleaning procedure, the Cu(111) surface exhibits a sharp ( $1 \times 1$ ) LEED pattern. The AES measurement indicates that the Ar-Ne mixture is effective for removing carbon, sulfur and oxygen contaminants from the surface to below the detection limit of the AES system. The substrate is flash-heated to 500 K right before each experiment. Using a combination of an electron beam heater and a close-cycle helium refrigerator (CYROMECH GB220), we control the substrate temperature from 33 to 1500 K. The temperature is monitored with a Type-E thermocouple attached to the side of the Cu substrate. The thermocouple reading is referenced to a junction submerged in liquid nitrogen.

The chamber is specially equipped with a CreaTec Fischer Atomizer (HLC-40-200). It consists of a 0.5 mm diameter tungsten filament coil mounted inside 1 cm diameter  $\times$  5 cm long molybdenum tube. Through a leak valve, molecular hydrogen gas flows through the molybdenum tube before entering the chamber. The tungsten filament is heated with a programmable current supply to a controllable temperature

from 300 to 2800 K. The filament temperature  $T_f$  is monitored, as the feedback to the programmable filament current supply, with a type-C thermocouple (W + 5%Re/W + 26%Re) placed 1 ~ 2 mm from the filament. The orifice of the molybdenum tube from which the heated molecular hydrogen gas emerges is 18 cm from the Cu sample and points at the sample at an angle of  $42^\circ$ . The orifice is also in the line of sight of (and at a distance 12 cm from) the head of the quadrupole mass spectrometer. By measuring the ion current at atomic mass unit (AMU) = 2 with the quadrupole mass spectrometer, we directly monitor the net partial pressure of hydrogen molecules, including those after collisions with the chamber walls. When molecular hydrogen gas enters the chamber through the atomizer with the filament temperature  $T_f$  set well below 2000 K, the gas is only heated close to  $T_f$  without measurable dissociation (fragmentation). When  $T_f$  is near or above 2000 K, a significant fraction of molecular hydrogen is dissociated into atomic fragments. We can determine the efficiency of fragmentation from the change in molecular hydrogen partial pressure upon the turn-on of the tungsten filament to a set temperature. In Fig. 1, we show the ion current at atomic mass unit (AMU) = 2 before and after the atomizer filament is turned on to  $T_f = 1973$  K. The molecular hydrogen partial pressure in the chamber drops from  $5.2 \times 10^{-7}$  Torr (when the filament is off) by 21%. Due to recombination in the chamber, the fraction of hydrogen molecules that are fragmented is higher than 21%. (One may increase the filament temperature beyond 1973 K until the molecular hydrogen pressure reaches the minimum value and apply the method of Eibl et al. to determine the fraction of dissociation [4]. We were not able to do so because operating the filament beyond 2000 K caused it to break up in our atomizer.) When  $T_f$  is reduced by 500 K, down to only 1473 K, we detect no change in the ion current at AMU = 2. This means that at this temperature the filament only heats up hydrogen molecules without dissociation.

For the adsorption experiment, the partial pressure of molecular hydrogen gas or of Xe gas in the chamber is monitored with a calibrated ionization gauge, and the readings are cor-

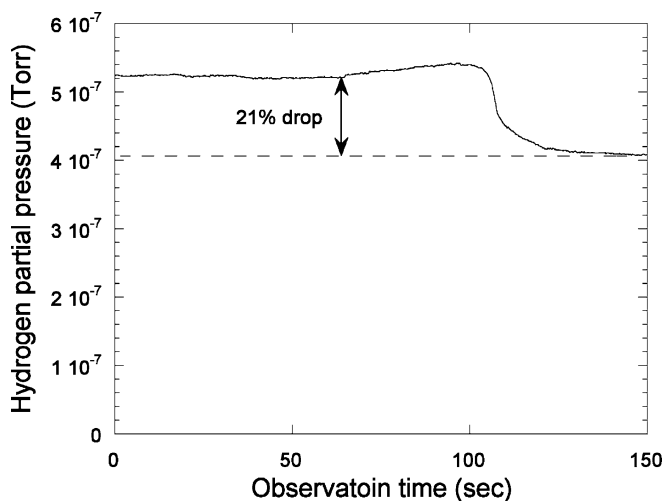


FIGURE 1 Change in molecular hydrogen partial pressure when the tungsten filament of the atomizer is turned on to a set temperature  $T_f = 1973$  K. The pressure drop (21% in the present case) is proportional to the cracking (fragmentation) efficiency of the atomizer at the set temperature

rected with the corresponding gas conversion factors. The exposure in units of Langmuir (Langmuir: 1 L =  $10^{-6}$  Torr s) is computed from the corrected partial pressure and the exposure time.

We use the oblique-incidence reflectivity difference (OI-RD) technique to monitor the adsorbate coverage in situ. OI-RD is a special form of polarization-modulated nulling ellipsometry. The details of the OI-RD setup and the operating procedures have been described elsewhere [25]. In the present experiment the probe laser is a 5 mW He-Ne laser at wavelength  $\lambda = 6328 \text{ \AA}$ , and is incident on the Cu(111) substrate at  $\varphi_{\text{inc}} = 66^\circ$ . Let  $r_{p0} = |r_{p0}| \exp(i\Phi_{p0})$  and  $r_{s0} = |r_{s0}| \exp(i\Phi_{s0})$  be the reflection coefficients for  $p$ - and  $s$ -polarized components of the incident laser beam off the bare substrate. Let  $r_p = |r_p| \exp(i\Phi_p)$  and  $r_s = |r_s| \exp(i\Phi_s)$  be the reflection coefficients from the substrate covered with adsorbates. Using the OI-RD technique, we directly measure the real and imaginary parts of the reflectivity difference defined as  $\Delta_p - \Delta_s \equiv \Delta \ln(r_p/r_s) = (r_p - r_{p0})/r_{p0} - (r_s - r_{s0})/r_{s0}$ . The real part,  $\text{Re}\{\Delta_p - \Delta_s\} = |r_p|/|r_{p0}| - |r_s|/|r_{s0}|$ , corresponds to differential magnitude change, while the imaginary part,  $\text{Im}\{\Delta_p - \Delta_s\} = (\Phi_p - \Phi_{p0}) - (\Phi_s - \Phi_{s0})$ , corresponds to differential phase change. Based on a classical three-layer model, the reflectivity difference is related to optical and structural properties of the substrate and the adsorbate overlayer by [4, 25, 26],

$$\Delta_p - \Delta_s \approx (-i) \frac{4\pi \cos \varphi_{\text{inc}} \sin^2 \varphi_{\text{inc}} \varepsilon_s}{(\varepsilon_s - 1)(\varepsilon_s \cos^2 \varphi_{\text{inc}} - \sin^2 \varphi_{\text{inc}})} \times \frac{(\varepsilon_d - \varepsilon_s)(\varepsilon_d - 1)}{\varepsilon_d} \left(\frac{d}{\lambda}\right) \left(\frac{\theta}{\theta_s}\right), \quad (1)$$

where  $\varepsilon_s$  is the bulk optical dielectric constant of the substrate. For Cu(111), we have determined independently from a grating-coupled surface-plasmon resonance excitation measurement that  $\varepsilon_s(632.8 \text{ nm}) = -9.53 + i0.142$ .  $\varepsilon_d$  is the effective optical dielectric constant of the adsorbate-modified surface layer including a saturated adsorbate monolayer.  $d$  is the effective thickness of the adsorbate-modified surface layer.  $\theta$  is the coverage of adsorbates defined as the ratio of the surface density of adsorbates to that of the top-most substrate atoms.  $\theta_s$  is the saturation coverage that may vary with the condition of exposure. The linear dependence of  $\Delta_p - \Delta_s$  on  $\theta$  has been shown to be a good approximation for hydrogen and Xe on Ni(111) (a closed-packed surface similar to Cu(111)) [3]. By monitoring  $\Delta_p - \Delta_s$ , we follow the evolution of the adsorbate coverage.

We note that depending on the substrate and the wavelength, one type of adsorbates may induce primarily a differential magnitude change, while another type of adsorbate may only cause a differential phase change. As we will show, adsorption of Xe atoms on Cu(111) only leads to a differential phase change at the He-Ne wavelength, while adsorption of hydrogen atoms on Cu(111) primarily induces a differential magnitude change. Such dramatically different responses are useful when we study coadsorption of hydrogen and Xe on Cu(111). The capability of measuring both the real and imaginary parts of  $\Delta_p - \Delta_s$  makes the OI-RD technique more versatile than optical second-harmonic gener-

ation (SHG) [27] and work function techniques. Physisorbed molecules or atoms neither directly nor indirectly change the second-order optical nonlinearity of a substrate surface, rendering the SHG technique insensitive to physisorption [28]. In comparison, a layer of physisorbed species always induces a significant differential phase change that is easily detected in an OI-RD measurement. The work function technique is sensitive to both physisorbed and chemisorbed species on a surface [29]. However being a single-value technique, when two different species co-adsorb on a surface, the work function technique cannot be used to separate contributions from each of the co-adsorbed species in order to determine the respective coverages. In contrast, being a two-parameter technique, the OI-RD technique alone can be used to determine the coverage of two co-adsorbed species on a surface based on a simultaneous measurement of the real and imaginary parts of  $\Delta_p - \Delta_s$ .

### 3 Results and discussion

#### 3.1 Adsorption of room-temperature and hot hydrogen molecules on Cu(111)

We first checked the adsorption of room-temperature hydrogen molecules on Cu(111) by back-filling the chamber with a  $5.2 \times 10^{-7}$  Torr hydrogen gas. The substrate was at 100 K. From a complete lack of change in  $\Delta_p - \Delta_s$ , we conclude that the dissociation probability of room-temperature molecular hydrogen on Cu(111) is below the detection limit of our present experiment, reaffirming that molecular hydrogen adsorption on Cu(111) requires overcoming an activation barrier. Molecular hydrogen does not physisorb on Cu(111) at 100 K either.

We next investigated the adsorption of filament-heated hydrogen molecules on Cu(111) at 100 K. The chamber is back-filled with a steady flow of molecular hydrogen through the atomizer to a partial pressure of  $5.2 \times 10^{-7}$  Torr. We then turn on the atomizer filament to  $T_f = 1473 \text{ K}$ . With the quadrupole mass analyzer set at atomic mass unit (AMU) = 2, we detect no change in hydrogen partial pressure, indicating that the heated molecular hydrogen gas is not fragmented at 1473 K. In Fig. 2, we show the measured  $\Delta_p - \Delta_s$  during the process. Both the real and imaginary parts of  $\Delta_p - \Delta_s$  change in response to exposure of hot molecular hydrogen, and reach their respective saturation levels.  $\text{Re}\{\Delta_p - \Delta_s\}$  is most prominent. The optical data show that a noticeable fraction of the hot molecular hydrogen is dissociated into atomic fragments upon impinging on Cu(111), and the atomic hydrogen become adsorbed. The dissociative adsorption reaches a saturation level. We see no evidence of the hydrogen adatoms being absorbed into the bulk. Based on the work of Anger and coworkers, we expect the saturation coverage in our case to be  $\theta_s = 0.5$  [11].

We can further deduce the adsorption kinetics. Knowing that  $\text{Re}\{\Delta_p - \Delta_s\}$  varies linearly with atomic deuterium coverage on Ni(111) (a surface structurally similar to Cu(111)) through a calibration against thermal desorption yields [3], we assume here that  $\text{Re}\{\Delta_p - \Delta_s\}$  from Cu(111) also varies linearly with atomic hydrogen coverage as predicted by (1). We can then determine the hydrogen adatom coverage during exposure by computing the ratio of  $\text{Re}\{\Delta_p - \Delta_s\}$  in Fig. 2 to its saturation value of 0.0061 and multiplying the ratio by  $\theta_s = 0.5$ . In Fig. 3, we plot the atomic hydrogen cover-

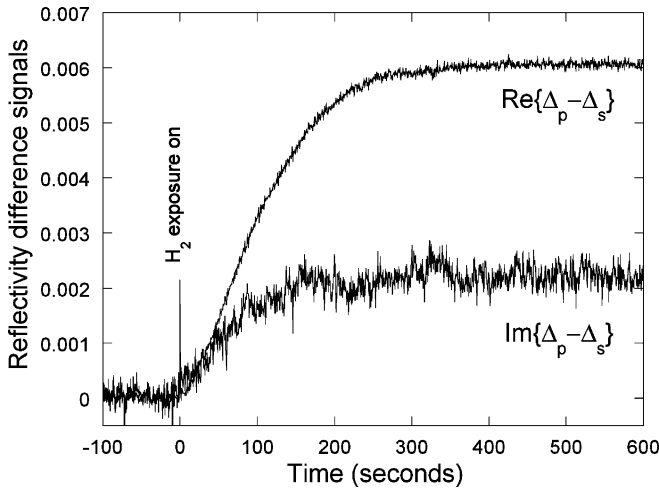


**FIGURE 2** Reflectivity difference signals  $\Delta_p - \Delta_s$  from Cu(111) vs. time when exposed to tungsten-filament-heated hydrogen molecules at a pressure of  $5.2 \times 10^{-7}$  Torr. The Cu(111) substrate is held at 100 K. The tungsten filament is set to 1473 K

age versus the hot molecular hydrogen exposure. The uptake curve cannot be described by a Langmuir kinetic over the entire range of the coverage. Instead, up to  $\theta = 0.25$  where adsorbed hydrogen atoms can form the  $p(2 \times 2)$  over-structure, the coverage increases linearly with the exposure (shown in solid circles), indicating that hot hydrogen molecules dissociate and adsorb on Cu(111) with a constant sticking probability  $S_0 = 0.0062$ . From  $\theta = 0.25$  up to 0.5 where adsorbed hydrogen atoms form three equivalent domains of the  $(1 \times 2)$  over-structure [30], further dissociative adsorption of hot hydrogen molecules follows a Langmuir kinetic (shown in open circles) with a coverage-dependent sticking probability  $S'_0 [1 - (\theta - 0.25)/(\theta_s - 0.25)]$ . The initial sticking probab-

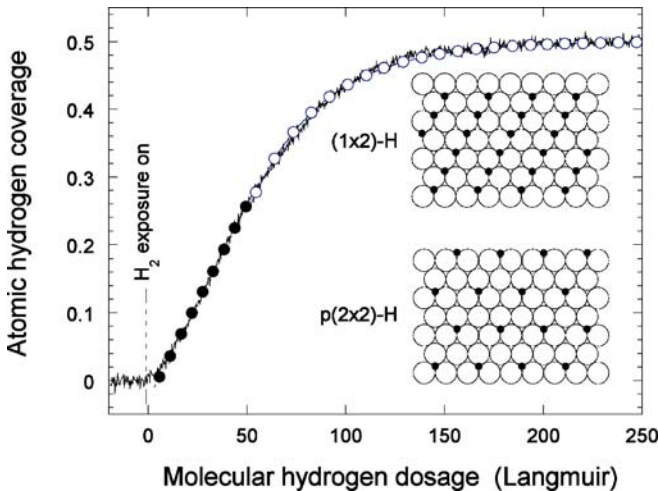


**FIGURE 3** Atomic hydrogen coverage on Cu(111) vs. exposure of filament-heated hydrogen molecules. The substrate is held at 100 K. The tungsten filament is again set to 1473 K. From  $\theta = 0$  to 0.25 (where hydrogen adatoms form a  $p(2 \times 2)$  over-structure), the coverage increases linearly with exposure, indicating that the hot hydrogen molecules adsorb with a constant sticking probability  $S = 0.0062$ . From  $\theta = 0.25$  to 0.5 (where hydrogen adatoms form three equally probable  $(1 \times 2)$  over-structures [30]), the further adsorption of hot hydrogen molecules follows a Langmuir kinetic with an initial sticking probability of  $S_0 = 0.0074$

ity in this coverage range is determined to be  $S'_0 = 0.0074$ . In arriving at the sticking probabilities, we have assumed that 100% of the hydrogen molecules are excited to the filament temperature, which leads to over-estimates of the sticking probabilities. It is noteworthy though that our findings agree well with the mono-energetic molecular beam study reported by Anger and coworkers [11].

### 3.2 Isothermal desorption of hydrogen adatoms from Cu(111)

We studied the isothermal desorption of hydrogen adatoms from Cu(111) between 270 and 330 K. The procedure is as follows. At a fixed substrate temperature, we expose Cu(111) to hot molecular hydrogen (with the atomizer filament set at 1473 K and a partial pressure at  $5.2 \times 10^{-7}$  Torr) until a steady-state initial coverage is reached. We then quickly turn off the atomizer filament and follow the coverage of hydrogen adatoms with the OI-RD technique as the desorption proceeds.

In Fig. 4 we display the desorption isotherms of hydrogen adatoms obtained at various temperatures between 270 and 330 K. Since the desorption of hydrogen adatoms is associative, we expect the rate to follow a second-order equation [1,8],

$$\frac{d\theta}{dt} = - \left( \frac{2\nu_d(T)}{\theta_s} \right) \theta^2 \quad (2)$$

where  $\nu_d(T)$  is the rate constant for the associative desorption. The factor of 2 comes from the fact that one associative desorption event succeeds at the expense of two hydrogen adatoms. Assuming that  $\nu_d(T)$  does not vary with the hydrogen adatom coverage significantly, (2) is easily solved by

$$\theta(t) = \frac{\theta(0)}{1 + (2\nu_d(T)\theta(0)/\theta_s)t} \quad (3)$$

Here  $\theta(0)$  is the initial coverage, and  $\theta_s = 0.5$ . We fit the experimental curves in Fig. 4 to (3) using  $\nu_d(T)$  as the only adjustable parameter (dotted lines in Fig. 4). We display the Arrhenius plot of  $\nu_d(T)$  in Fig. 5. The result is fit well (solid line

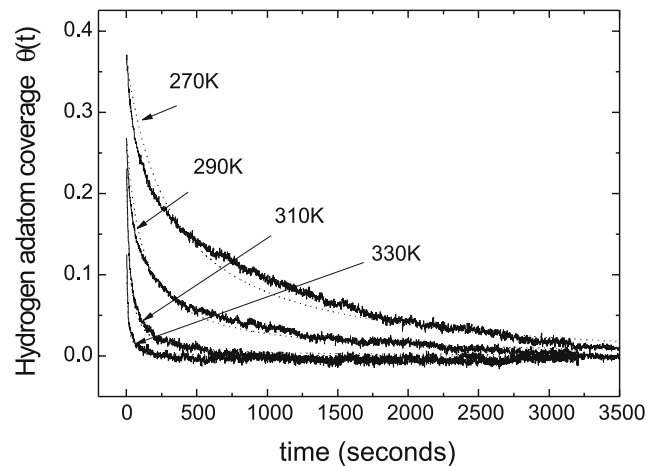


**FIGURE 4** Isothermal desorption of hydrogen adatoms from Cu(111) at different substrate temperatures. The *dashed lines* are fits to  $\theta(t) = \theta(0)/[1 + (2\nu_d(T)\theta(0)/\theta_s)t]$  with  $\nu_d(T)$  as the adjustable parameter (see the main text)

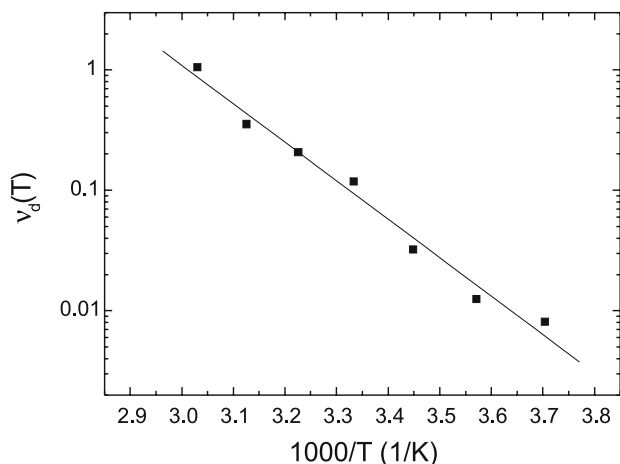


**FIGURE 5** Arrhenius plot of desorption rates  $\nu_d(T)$  for hydrogen adatoms on Cu(111). The fit (shown as the *solid line*) to  $\nu_d(T) = \nu_{d0} \exp(-E_{\text{des}}/k_B T)$  yields  $E_{\text{des}}(\text{H}/\text{Cu}(111)) = 0.63 \text{ eV}$  and  $\nu_{d0}(\text{H}/\text{Cu}(111)) = 1 \times 10^9 / \text{s}$

in Fig. 5) to an Arrhenius function of temperature,  $\nu_d(T) = \nu_{d0} \exp(-E_{\text{des}}/k_B T)$ . We find the activation energy and the pre-exponential factor for associative desorption of hydrogen adatoms from Cu(111) to be  $E_{\text{des}}(\text{H}/\text{Cu}(111)) = 0.63 \text{ eV}$  and  $\nu_{d0}(\text{H}/\text{Cu}(111)) = 1 \times 10^9 / \text{s}$ , respectively. These parameters compare well with the results reported by Anger and coworkers [11].

### 3.3 Adsorption of filament-heated molecular hydrogen on Xe-covered Cu(111)

The activated nature of molecular hydrogen adsorption is further manifested by exposing hot hydrogen molecules to Cu(111) that is pre-covered with a saturated monolayer of Xe atoms. In order for a hydrogen molecule to adsorb on 1-ML Xe/Cu(111) that blocks its adsorption site, it must displace Xe adatoms to make room for itself or for subsequently arrived hydrogen molecules. Consequently hot hydrogen molecules (obtained by passing through the 1473 K tungsten filament) will need to spend a significant fraction of its translational and internal energy to displace Xe adatoms on Cu(111). In doing so, the residual available energy of the molecule will not be enough to overcome the dissociation barrier on Cu(111) so that the net sticking probability is reduced dramatically. This is what we observed.

We deposit one monolayer of Xe on Cu(111) at 60 K by back-filling the chamber with the rare gas at a partial pressure of  $3 \times 10^{-8}$  Torr. At 60 K, our LEED measurement shows that one saturated monolayer of Xe adsorbs at on-top sites on Cu(111) and forms a commensurate, close-packed ( $\sqrt{3} \times \sqrt{3}$ )  $R30^\circ$  over-structure as shown in the insert in Fig. 6 [25].  $\Delta_p - \Delta_s$  in response to Xe adsorption are also shown in Fig. 6. In contrast to Fig. 2, only  $\text{Im}\{\Delta_p - \Delta_s\}$  responds to adsorption of Xe atoms on Cu(111). The footprint of a saturated Xe monolayer in ( $\sqrt{3} \times \sqrt{3}$ )  $R30^\circ$  structure blocks all 3-fold hollow sites for hydrogen adatoms. To examine such a blocking effect quantitatively, we exposed the Xe-covered Cu(111) to hot molecular hydrogen gas at  $5.2 \times 10^{-7}$  Torr with the atomizer filament again set at 1473 K. In Fig. 7 we show the hydrogen adatom adsorp-

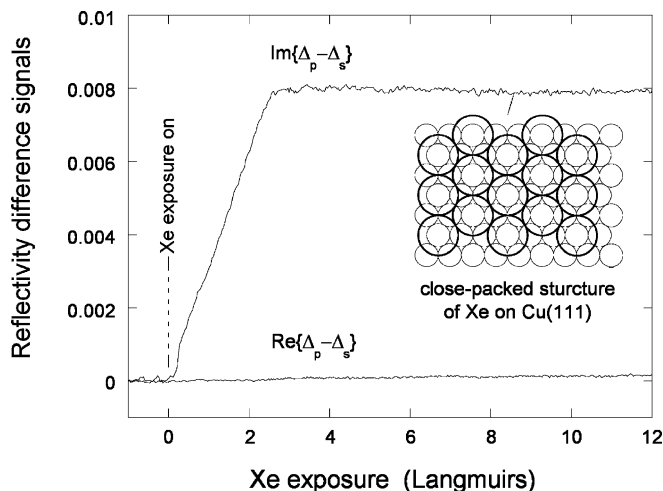


**FIGURE 6** Reflectivity difference signals,  $\Delta_p - \Delta_s$ , from Cu(111) vs. exposure of Xe at a partial pressure  $3 \times 10^{-8}$  Torr. The substrate is at 60 K. The saturation in  $\text{Im}\Delta_p - \Delta_s$  marks the completion of a full monolayer of Xe atoms on Cu(111), in the form of a close-packed structure. By occupying on-top sites, the foot-prints of Xe adatoms (large open circles with the Van der Waals radius of a Xe atom) completely block 3-fold hollow sites for hydrogen adsorption

tion isotherm (monitored with  $\text{Re}\{\Delta_p - \Delta_s\}$ ) on the Xe-covered Cu(111). After 160 L, the hydrogen adatom coverage on 1ML-Xe/Cu(111) only increased from 0 to 0.02. This shows that the pre-adsorbed Xe monolayer indeed inhibits subsequent dissociative adsorption of filament-heated hydrogen molecules. In our case it reduces the sticking probability of hot hydrogen molecules by more than a factor of 20.

The “blocking” effect of a pre-adsorbed Xe monolayer can be exploited for spatial patterning of hydrogen adatom density profiles on Cu(111) and on other Cu substrates. Williams and coworkers were the first to recognize and demonstrate the usefulness of physisorbed monolayer templates for spatial

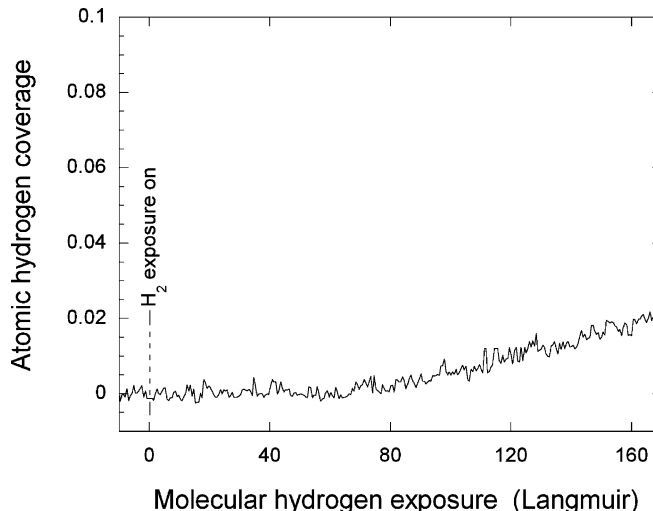


**FIGURE 7** Adsorption isotherm of filament-heated hydrogen molecules on Xe-covered Cu(111). The substrate is held at 60 K. The tungsten filament  $T_f$  is at 1473 K. After an exposure of 160 L, the hydrogen adatom coverage only increases by 0.02, indicating that the sticking probability is reduced by a factor of 20

patterning of strongly bonded adsorbates on Si [28]. Periodic density profiles of hydrogen adatoms have been used for studying classical and quantum diffusion of light adatoms on metals. Adsorbate density or coverage gratings are preferably formed using the method of pulsed laser-induced thermal desorption (LITD) with interference patterns of nanosecond optical pulses [15, 20, 31, 32]. For metal substrates, the choice of nanosecond optical pulses (with duration  $\tau_p \sim 10$  ns) for thermal desorption ensures that thermal diffusion lengths, varying as  $\propto \sqrt{\tau_p}$ , are less than spatial periods of adsorbate density gratings so that the latter have sufficient contrasts. As pointed out by Williams et al., significant thermal desorption of strongly bonded adsorbates with nanosecond optical pulses may require the peak surface temperature during desorption too close to or over the melting point of the substrate and thus cause undesirable optical damage. Indeed for hydrogen adatoms on Cu(111) with a desorption activation energy  $E_{\text{des}}(\text{H}/\text{Cu}(111)) = 0.63$  eV and a pre-exponential factor  $\nu_{\text{d0}}(\text{H}/\text{Cu}(111)) = 1 \times 10^9$  /s, the peak surface temperature needed to remove 50% of hydrogen adatoms in 10 nanoseconds is 1500 K, over the melting point of 1358 K for Cu. Since a pre-adsorbed Xe monolayer blocks the dissociative adsorption of hydrogen on Cu(111), one can form periodic density profiles of Xe adatoms on Cu(111) first and use it as the template to form periodic density profiles of hydrogen adatoms by exposing Xe-covered Cu(111) to hot molecular hydrogen [33]. In Fig. 8, we display the desorption isotherms of Xe adatoms from Cu(111) obtained at various temperature between 69 and 77 K. The desorption rate is a function of temperature and yet is independent of Xe coverage because the Xe coverage decreases linearly with time at a fixed temperature. Knowing that the saturation coverage of Xe on Cu(111) is  $\theta_{\text{Xe},s} = 1/3$ , the Xe coverage as a function of time can be expressed as  $\theta_{\text{Xe}}(t) = \theta_{\text{Xe},s}(1 - \nu_{\text{d}}(T)t)$ . Equivalently, the normalized Xe coverage can be expressed as  $\theta_{\text{Xe}}(t)/\theta_{\text{Xe},s} = 1 - \nu_{\text{d}}(T)t$ . This desorption behavior is the same as that of Xe on Ni(111), Cu(100), graphite (0001), and W(110), and can be explained by a model proposed by Bienfait and Venables [3, 34–39]. By fitting the normalized

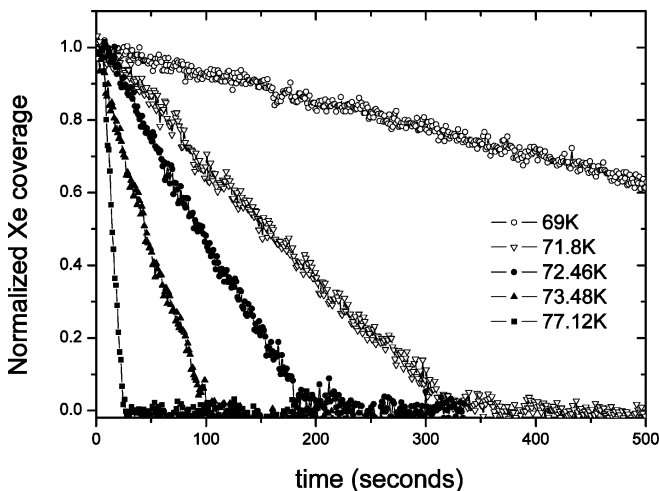


**FIGURE 8** Desorption isotherms of the Xe monolayer on Cu(111) at different substrate temperatures. The desorption rates are independent of Xe coverage

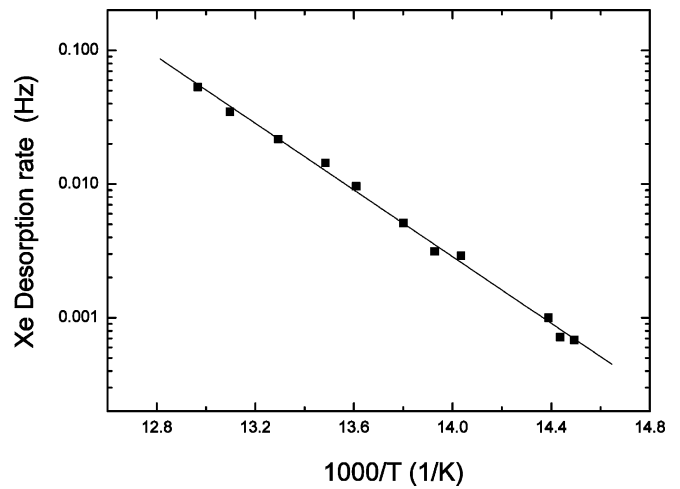


**FIGURE 9** Arrhenius plot of the desorption rate constant  $\nu_{\text{d}}(T)$  for the Xe monolayer on Cu(111). The fit to  $\nu_{\text{d}}(T) = \nu_{\text{d0}} \exp(-E_{\text{des}}/k_{\text{B}}T)$  (shown as a solid line) yields  $E_{\text{des}}(\text{Xe}/\text{Cu}(111)) = 0.25$  eV and  $\nu_{\text{d0}}(\text{Xe}/\text{Cu}(111)) = 8.2 \times 10^{14}$  /s

Xe coverage to  $1 - \nu_{\text{d}}(T)t$  at different substrate temperatures, we obtain the desorption rate  $\nu_{\text{d}}(T)$  as a function of  $T$ . In Fig. 9, we display the Arrhenius plot of  $\nu_{\text{d}}(T)$ . The experimental values of  $\nu_{\text{d}}(T)$  fit well to an Arrhenius function  $\nu_{\text{d}}(T) = \nu_{\text{d0}} \exp(-E_{\text{des}}/k_{\text{B}}T)$ . From the fit, we determined the desorption activation energy for Xe adatoms to be  $E_{\text{des}}(\text{Xe}/\text{Cu}(111)) = 0.25$  eV and the preexponential factor to be  $\nu_{\text{d0}}(\text{Xe}/\text{Cu}(111)) = 8.2 \times 10^{14}$  /s. The peak surface temperature needed to remove 50% of Xe adatoms in 10 ns is only 170 K, far below the melting point of Cu. Xe templates can be subsequently removed by laser-induced thermal desorption, leaving behind a hydrogen density grating on Cu(111) more or less undisturbed. The excess energy released during the dissociation of a hydrogen molecule on Cu(111) may enable the atomic hydrogen to migrate along the surface by more than one lattice constant (transient mobility). For density profiles with spatial periods in the range of microns, this transient mobility effect does not noticeably change the definition of originally patterned density profiles.

#### 4 Conclusion:

We investigated the dissociative adsorption and associative desorption of hydrogen on Cu(111). We found that hot molecular hydrogen gas heated with a 1473 K tungsten filament is energetic enough to dissociate and become adsorbed on Cu(111), while little dissociative adsorption is observed for room-temperature molecular hydrogen. Up to  $\theta = 0.25$ , the sticking probability for the 1473 K-filament-heated hydrogen molecules is constant,  $S_0 = 0.0062$ . From  $\theta = 0.25$  to the saturation coverage of  $\theta_s = 0.5$ , further dissociative adsorption follows a Langmuir kinetic with a coverage dependent sticking probability of  $0.0074 \times [1 - (\theta - 0.25)/(\theta_s - 0.25)]$ . The isothermal desorption of hydrogen adatoms from 270 to 330 K obeys a second-order kinetic with activation energy of 0.63 eV and a pre-exponential factor of  $1 \times 10^9$  /s. We also found that the adsorption of hydrogen is blocked effectively by a pre-adsorbed monolayer of Xe atoms on Cu(111). Physisorbed Xe monolayers can be used as masks for spatial

patterning of hydrogen adatom density on Cu(111) and other Cu surfaces.

**ACKNOWLEDGEMENTS** This work is supported by the donors of the Petroleum Research Fund, administered by the American Chemical Society, and in part by the Chinese Natural Science Foundation and the Chinese Academy of Sciences.

## REFERENCES

- 1 K. Christmann, O. Schober, G. Ertl, M. Neumann, *J. Chem. Phys.* **60**, 4528 (1974)
- 2 K. Christmann, R.J. Behm, G. Ertl, M.A. Van Hove, W.H. Weinberg, *J. Chem. Phys.* **70**, 4168 (1979)
- 3 A. Wong, X.D. Zhu, *Appl. Phys. A* **63**, 1 (1996)
- 4 C. Eibl, G. Lackner, A. Winkler, *J. Vac. Sci. Technol. A* **16**, 2979 (1998)
- 5 D.O. Hayward, B.M. Trapnell, *Chemisorption* (Butterworths, London, 1964), p. 75
- 6 M. Balooch, M.J. Cardillo, D.R. Miller, R.E. Stickney, *Surf. Sci.* **46**, 358 (1974)
- 7 B.E. Hayden, C.L.A. Lamont, *Phys. Rev. Lett.* **63**, 1823 (1989)
- 8 B.E. Hayden, C.L.A. Lamont, *Chem. Phys. Lett.* **160**, 331 (1989)
- 9 C.T. Rettner, D.J. Auerbach, H.A. Michelsen, *Phys. Rev. Lett.* **68**, 1164 (1992)
- 10 D.J. Auerbach, C.T. Rettner, H.A. Michelsen, *Surf. Sci.* **283**, 1 (1993)
- 11 G. Anger, A. Winkler, K.D. Rendulic, *Surf. Sci.* **220**, 1 (1989)
- 12 J.L.F. Da Silva, C. Stampfl, M. Scheffler, *Phys. Rev. Lett.* **90**, 066104 (2003)
- 13 R. DiFoggio, R. Gomer, *Phys. Rev. B* **25**, 3490 (1982)
- 14 T.-S. Lin, R. Gomer, *Surf. Sci.* **255**, 41 (1991)
- 15 X.D. Zhu, A. Lee, A. Wong, U. Linke, *Phys. Rev. Lett.* **68**, 1862 (1992)
- 16 L.J. Lauhorn, W. Ho, *Phys. Rev. Lett.* **85**, 4566 (2000)
- 17 C.P. Flynn, A.M. Stoneham, *Phys. Rev. B* **1**, 3966 (1970)
- 18 D. Emin, M.I. Baskes, W.D. Wilson, *Phys. Rev. Lett.* **42**, 791 (1979)
- 19 J. Kondo, in *Fermi Surface Effects*, Springer Series in Solid State Sciences Vol. 77, ed. by J. Kondo, A. Yoshimori (Springer-Verlag, Heidelberg, 1988), p. 1
- 20 G.X. Cao, E. Nabighian, X.D. Zhu, *Phys. Rev. Lett.* **79**, 3696 (1997)
- 21 F. Greuter, E.W. Plummer, *Solid State Commun.* **48**, 37 (1983)
- 22 G. Lee, D.B. Poker, D.M. Zehner, E.W. Plummer, *Surf. Sci.* **358**, 717 (1996)
- 23 G. Lee, E.W. Plummer, *Surf. Sci.* **498**, 229 (2002)
- 24 G. Comsa, R. David, *Surf. Sci.* **117**, 77 (1982)
- 25 P. Thomas, E. Nabighian, M.C. Bartelt, C.Y. Fong, X.D. Zhu, *Appl. Phys. A* **79**, 131 (2004)
- 26 X.D. Zhu, *Phys. Rev. B* **69**, 115407 (2004)
- 27 H.W.K. Tom, C.M. Mate, X.D. Zhu, J.E. Crowell, T.F. Heinz, G.A. Somorjai, Y.R. Shen, *Phys. Rev. Lett.* **52**, 348 (1984)
- 28 P.A. Williams, G.A. Reider, L. Leping, U. Höfer, T. Suzuki, T.F. Heinz, *Phys. Rev. Lett.* **79**, 3459 (1997)
- 29 A. Zangwill, *Physics at Surfaces* (Cambridge University Press, New York, 1988), p. 200
- 30 E.M. McCash, S.F. Parker, J. Pritchard, M.A. Chesters, *Surf. Sci.* **215**, 363 (1989)
- 31 X.D. Zhu, Th. Rasing, Y.R. Shen, *Phys. Rev. Lett.* **61**, 2883 (1988)
- 32 G.A. Reider, U. Höfer, T.F. Heinz, *Phys. Rev. Lett.* **66**, 1994 (1991)
- 33 Y.Y. Fei, X.D. Zhu, *Europhys. Lett.* (2006), in press
- 34 A. Glachant, U. Bardi, *Surf. Sci.* **87**, 187 (1979)
- 35 M. Bienfait, J.A. Venables, *Surf. Sci.* **61**, 667 (1976)
- 36 J. Suzanne, J.P. Coulomb, M. Bienfait, *Surf. Sci.* **44**, 141 (1974)
- 37 J. Suzanne, J.P. Coulomb, M. Bienfait, *Surf. Sci.* **47**, 204 (1975)
- 38 G. Quentel, J.M. Rickard, R. Kern, *Surf. Sci.* **50**, 343 (1975)
- 39 R. Opila, R. Gomer, *Surf. Sci.* **112**, 1 (1981)